EXPERIMENTS ON SLUG MIXING UNDER NATURAL CIRCULATION CONDITIONS AT THE ROCOM TEST FACILITY USING HIGH RESOLUTION MEASUREMENT TECHNIQUE AND NUMERICAL MODELING

S. Kliem, T. Höhne, U. Rohde, F.-P. Weiss

Forschungszentrum Dresden-Rossendorf, Institute of Safety Research

P.O.B. 510119, D-01314 Dresden, Germany

Abstract

ROCOM is a four-loop test facility for the investigation of coolant mixing in the primary circuit of pressurized water reactors. Recently, a new sensor was developed for an improved visualisation and quantification of the coolant mixing in the downcomer. This new sensor spans a dense measuring grid and covers nearly the whole downcomer. In the presented work, special emphasis was given to the comparison of the data of this sensor with the results of calculations using the CFD code ANSYS CFX. A coolant mixing experiment during natural circulation conditions has been conducted. The underlying scenario of this experiment is based on a boron dilution scenario following a SBLOCA event. The corresponding CFD code solution has been obtained using the Best Practice Guidelines. All main effects observed in the measurement are described by the calculation. The detailed comparison reveals that the calculation underestimates the coolant mixing inside the reactor pressure vessel.

The measurement data, boundary conditions of the experiment and facility geometry can be made available to other CFD code users for benchmarking.

1. INTRODUCTION

Boron 10 is added to the reactor coolant of a pressurized water reactor (PWR) to control reactivity. The forced coolant circulation during normal operation or natural circulation ensures that the boric acid is homogeneously distributed in the reactor coolant system so that the boron concentration is practically uniform. The possibility of coolant with a relatively low boron concentration collecting in localized areas of the RCS has been under discussion for several years now (Hyvärinen, 1993). Causes might be the injection of coolant with less boron content from interfacing systems (external dilution) or separation of the borated reactor coolant into highly concentrated and diluted fractions (inherent dilution). One of the discussed scenarios of the inherent dilution is connected with a small break loss of coolant accident (SBLOCA). During such a postulated event the single-phase flow natural circulation in one or more loops can interrupt. This could happen when the high pressure safety injection (HPSI) partly fails. In such cases, a part of the decay heat is removed from the core in the reflux-condensation mode. This leads to the production and accumulation of low borated coolant in the primary circuit, i.e. the above mentioned inherent dilution. Experimentally it has been shown, that the accumulation takes place in those loops not receiving ECC injection. The primary pressure further drops due to the inventory losses through the leak and due to the down cooling of the secondary side initiated simultaneously with the SCRAM after recognition of the leak. At a certain pressure level, the mass flow rate injected by the ECC systems will overcompensate the leakage losses. The primary system will be filled up again and single-phase natural circulation re-establishes. The one phase natural circulation forwards these under-borated slugs towards the reactor core. During the transport from the cold legs through the downcomer and the lower plenum, the slugs undergo a mixing with the ambient coolant in the reactor pressure vessel (RPV) and with the coolant from the loops with available ECC injection, both having a higher boron concentration. In such scenarios, the described slug mixing is the only mechanism mitigating the possible reactivity insertion into the core. The knowledge of the boron concentration distribution at the inlet and inside the reactor core is of primary importance for the assessment of the neutron kinetic core behaviour during such an accident.

At present time, this information is almost exclusively derived from experiments at coolant mixing test facilities.

The application of Computational Fluid Dynamics (CFD) simulation methods to model these single-phase flow phenomena is underway. In the near future, these codes are expected to be used for assessing nuclear reactor safety. This objective requires comprehensive validation work, which should be performed again dedicated experiments at test facilities providing the necessary detail of modelling all structures important for coolant mixing. This concerns the loop and vessel geometry and especially the internals of the RPV. Furthermore, the measurement data for the validation should be provided with high resolution in space and time to enable a detailed comparison with the calculation results.

The measurement technique at the Rossendorf Coolant Mixing (ROCOM) test facility has been improved recently in order to enable high-level CFD code validation.

A coolant mixing experiment during natural circulation conditions has been conducted. The initial and boundary conditions were derived from the above mentioned SBLOCA scenario.

2 THE ROCOM TEST FACILITY AND THE MEASUREMENT TECHNIQUE

2.1 ROCOM test facility

ROCOM is a four-loop test facility for the investigation of coolant mixing operated with water at room temperature (Hertlein, 2003; Prasser, 2003; Kliem, 2007). The facility models a KONVOI-type reactor with all details important for the coolant mixing along the flow path, from the cold-leg nozzles up to the core inlet, at a linear scale of 1:5. Special attention was given to components which significantly influence the velocity field, such as the core barrel with lower core support plate and core simulator, perforated drum in the lower plenum, and inlet and outlet nozzles. The geometry of the inlet nozzles, with their diffuser segments and the curvature radius of the inner wall at the junction with the RPV were modelled in detail. The core and the upper plenum were modelled in a very simplified manner. Individually controllable pumps in each loop give the possibility to perform tests over a wide range of flow conditions, from natural circulation to nominal flow rate, including flow ramps (pump and natural circulation start-up). The water inventory of the loops was kept to the scale of 1:125, and the travelling time of the coolant was identical to that of the original reactor.

2.2 Measurement technique

The facility is operated with de-mineralized water at room temperature. Salt water or brine is used to alter the local electrical conductivity of the fluid in order to label a specific volume of water and thus simulate an under-borated slug of coolant. The distribution of this tracer in the test facility is measured by special wire-mesh electrical conductivity sensors developed by FZD, which allow a high-resolution measurement of the transient tracer concentration with regard to space and time (Prasser, 1998). These wire mesh sensors consist of two planes of electrodes, where the mesh spans the flow cross-section. The measurement of the instantaneous local conductivity of the medium is realized in the vicinity of each crossing point of two perpendicular wires. These measured local conductivities, which can be recorded with a frequency of up to 1000 Hz and are subsequently compared to reference values in order to estimate the position of the under-borated slugs and its transport. The result is a dimensionless mixing scalar $\Theta_{x,y,z}(t)$ that characterizes the instantaneous share of the coolant originating from the labelled volume (under-borated slug) at a given position inside the flow field. It is calculated by relating the local instantaneous conductivity $\sigma_{x,y,z}(t)$ to the amplitude of the conductivity change at the reference position σ_1 (usually the labelled slug in the cold leg) according to the following formula:

$$\Theta_{x,y,z}(t) = \frac{\sigma_{x,y,z}(t) - \sigma_0}{\sigma_1 - \sigma_0} \tag{1}$$

The lower reference value σ_0 is the initial conductivity of the water in the test facility before the experiment is started.

The transport of boron with the coolant can be described by the transport equation for a scalar. A scalar is a quantity, spread by fluid convection and diffusion without feedback from the scalar concentration to the fluid properties such as density or viscosity. In the test facility as well as in the original reactor, the flow is considered turbulent. Therefore, in applying the scalar under conditions of turbulent flow regimes, scalar transport is determined by turbulent dispersion, where the corresponding molecular diffusion of the boron plays a secondary role. Therefore, it is possible to reconsider the mixing of boron as that of an inert tracer, which is dissolved in the coolant of the test facility in much the same manner as the boron is dissolved in the coolant of the original reactor. Based on this similarity, the distribution of the boron concentration can be derived on the basis of the mixing scalar using:

$$C_B(x, y, z, t) = \Theta(x, y, z, t) \cdot (C_{B,1} - C_{B,0}) + C_{B,0} \qquad (2)$$

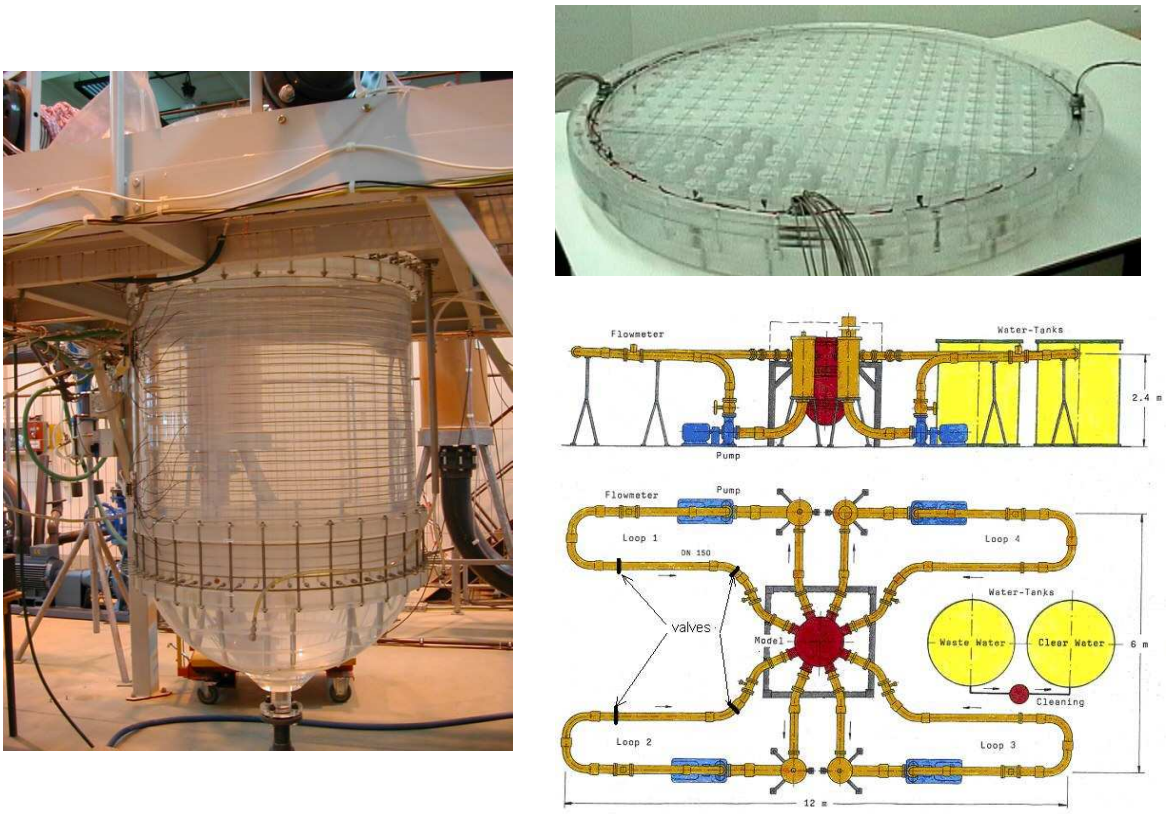

Fig. 1: View of the test facility with sensor in the downcomer, photo of the core inlet plane with integrated sensor and schematic of the test facility with position of the gate valves

All inlet nozzles can be equipped with sensors. Further, sensors can be installed at important positions along the flow path in the primary coolant loops (e.g. at the position of the ECC water injection). One sensor is integrated into the lower core support plate providing one measurement position at the entry into each fuel assembly (Fig. 1). For the experiments described in (Kliem, 2008a), a sensor was developed for an improved visualization and quantification of the coolant mixing in the downcomer. This new sensor replaces the two radial sensors being installed at the inlet and the outlet of the downcomer. It now spans a measuring grid of 64 azimuthal and 29 axial positions over the height of the downcomer (Fig. 1). For that purpose, 64 fixing bolts were attached to the inlet and the outlet flanges of the vertical section of the downcomer and between the bolts, 64 wires were fastened in order for the wires to cover entire length of the downcomer. Note that these wires are the transmitter electrodes. The receiver electrodes are made from strips of steel that are 3 mm wide, which are glued

onto the inner side of the vessel at a distance of 31 mm from each other over the length of the downcomer. The vertical wires are located near to the core barrel wall. In this way, the signal measured is the conductivity that is averaged over the width of the downcomer. This new sensor with its approximately 1900 single measurement positions allows obtaining a complete picture of the transient mixing processes in the downcomer. Comparison with the results of CFD calculations can be carried out on a qualitatively new level.

3 DESCRIPTION OF THE EXPERIMENT

Based on the above discussed scenario an experiment was set up at the ROCOM test facility. The boundary conditions on both slug volume and initial distance from the RPV have been derived from experiments on the formation and accumulation of under-borated slugs conducted at the thermal hydraulic test facility PKL (Mull, 2003). The mentioned experiments have shown that the natural circulation in the single loops restarts with a certain time delay between the loops after refilling of the primary circuit. The volumes of the accumulated under-borated coolant as well as the mass flow curves in the single loops differ also from each other. According to the experiments, accumulation of under-borated coolant takes place only in those loops, not receiving ECC injection.

As far as the experiment is dedicated to the CFD code validation, the boundary conditions have been simplified. Two neighbouring loops 1 and 2 (Fig. 1) of the test facility were equipped with pairs of fast acting gate valves. The volume between the valves in each loop constitutes a value of 57.6 l corresponding to a volume of 7.2 m^3 at the real plant. This is the volume of the loop seal and a part of the steam generator outlet chamber. The valve nearest to the RPV is located in a distance of 1.80 m from the cold leg outlet nozzle, which corresponds to the distance from the loop seal to the RPV.

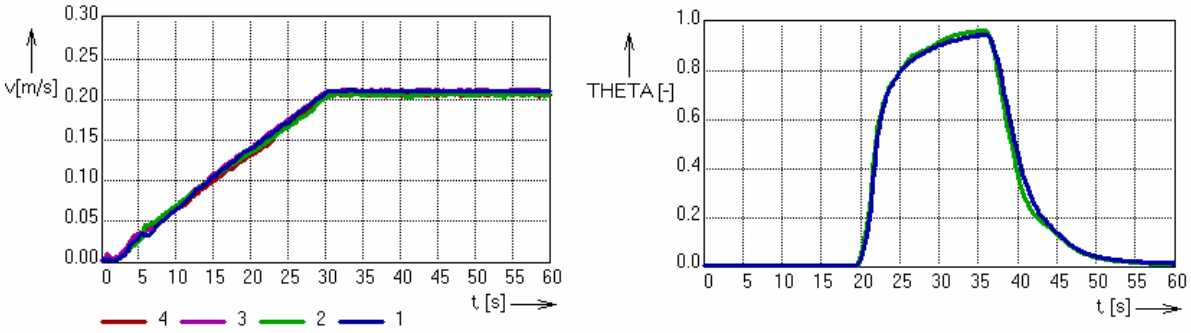

Fig. 2: Velocity ramp in all loops (left) and time history of the mixing scalar at the cold leg outlet nozzles in loop 1 and 2 (right) during the experiment (used as boundary conditions for the calculations)

The restart of the natural circulation is simulated by linear frequency ramps from zero to a value corresponding to a velocity value of 7 % of the nominal velocity in the loops. The time of increasing the flow rate is 30 s, identical frequency curves have been used in all four loops. The resulting velocity curves in the loops are shown on the left part of Fig. 2. The gate valves are closed in the initial state. Between them, under-borated slugs are prepared. The density of the under-borated slugs has not been adjusted; it is identical to the density of the coolant in the other parts of the facility. The experiment starts with the opening of the gate valves. The further actions are listed in Tab. 1.

Tab. 1: Sequence of the ROCOM experiment

Time [s]	**Action**
-3.0	Opening of the gate valves
0.0	Valves are fully open/ Start of the frequency ramp
30.0	Final value of frequency ramp reached
120.0	End of the experiment

The experiment has been carried out twelve times with identical boundary conditions. For the comparison with the calculations the measured data have been converted into mixing scalars according to Eq. (1). Further, the data at each measurement position have been averaged. These averaged data are the basis for a comparison with the calculation. The measured and averaged data from the sensors in the cold leg outlet nozzles of the two loops with the slugs are shown on Fig. 2 (right part).

An error analysis of the wire-mesh sensor data has been presented in (Kliem, 2008). It was shown that the mixing scalar can be determined with an error band of less than ± 3 %.

4. NUMERICAL MODELING WITH ANSYS CFX

The CFD code for simulating the mixing studies was CFX-11 (CFX11, 2007). CFX-11 is an element-based finite-volume method with second-order discretisation schemes in space and time. It uses a coupled algebraic multigrid algorithm to solve the linear systems arising from discretisation. The discretisation schemes and the multigrid solver are scalably parallelized. CFX-11 works with unstructured hybrid grids consisting of tetrahedral, hexahedral, prism and pyramid elements.

Discretisation errors can be reduced by using finer grids, higher-order discretisation methods and smaller time step sizes. However, in many practical three-dimensional applications grid- and time step-independent solutions cannot be obtained because of hardware limitations. In these cases, the remaining errors and uncertainties should be quantified as described in the ECORA Best Practice Guidelines (BPG) by Menter (2002).

4.1 Application of the Best Practice Guidelines for CFD

The application of the guidelines and procedures described in the BPG is especially important for the validation of CFD codes for nuclear reactor safety as there must be a strong emphasis on reliability and quality of the computational results. Reactor safety-critical flows are a special challenge for CFD simulations due to the complex geometry and transient flow conditions in real reactor scenarios that require very large computing resources.

The Best Practice Guidelines divide the different types of errors in CFD simulations into the two main categories:

- Numerical errors, caused by the discretisation of the flow geometry and the model equations, and by their numerical solution
- Model errors, which arise from the approximation of physical processes by empirical mathematical models

The BPG are built on the concept of an error hierarchy. This concept implies that numerical errors are quantified and reduced to an acceptable level, before comparison with experimental data is made. The separation of numerical errors from model errors then allows valid conclusions on model performance. The types of procedures and advice provided in the BPGs for performing CFD simulations are as follows: The first step was the selection of representative and solution-sensitive target variables: the additional scalar variable Mixing Scalar (Figs. 4, 5). This target variable was monitored. The convergence criterion was set low enough so that the target variable is no longer affected by it. Then the discretisation errors were quantified by performing time-step and grid refinement. At this stage, the numerically certified solution can be compared with experimental data. The remaining differences are the model errors. They can only be reduced by applying more accurate models.

Sensitivity tests for the following aspects were considered:

- Grid
    - Grid type and size,
    - outlet boundary position,
    - internal geometry

- Time-step size
- Turbulence model

Summaries of how these sensitivity tests were made are presented below.

4.1.1 Grid

Grid 1: Tetra Mesh		**Grid 2: Hybrid Mesh**	
RPV	Horizontal cut: Inlet nozzle plane	RPV	Horizontal cut: Inlet nozzle plane
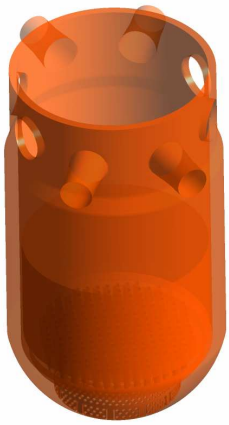		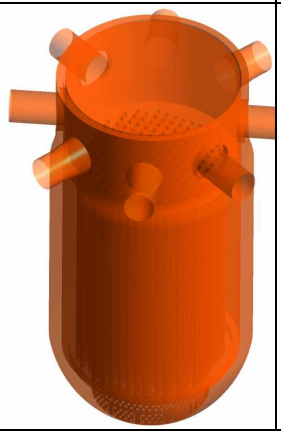	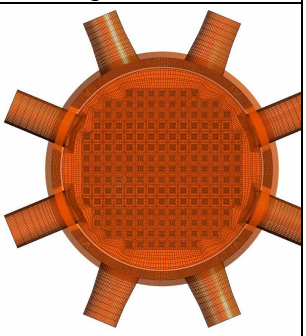

Fig. 3: Production meshes based on tetrahedral elements (left) and hybrid elements (right)

The aim was to make CFD calculations that gave grid-independent solutions, i.e. results that do not change when the grid is refined further. A grid-independent solution can be defined as a solution that has a solution error that is within a range that can be accepted by the end-user, in view of the purpose of the calculations.

Two different grid types were generated (Fig. 3), and the calculation results were compared with the experiment. Different features and also different mesh structures were used. However, it was noticed, that the grid generation consumes most of the work and a totally grid independent solution was not achieved.

Based on meshing studies in the FLOMIX-R project (Rohde, 2007), finally two grid types were used for the CFD calculations. They were called production meshes, because on the one hand, they allow getting the maximum correct results with minimum meshing efforts: the tetrahedral production mesh (grid 1) and the hybrid production mesh (grid 2). The production mesh is an optimum between maximum possible refined grids, but with omitting parts of the flow domain, which were found to be of small impact on the results, e.g. the cold leg loops. The production mesh is not yet a mesh, for which grid-independent solution was reached. In general, the choice of the production mesh is dependent on the process to be simulated.

On average the y+-values are in the downcomer y+= 65 for the tetrahedral mesh (grid 1) and y+= 29 for the hybrid mesh (grid 2). Both grid types are suitable for the post test calculation of ROCOM experiments. Because no full grid independence was achieved, there are differences in the results obtained with different mesh types like tetrahedral mesh and hybrid mesh (Fig. 4).

In the production meshes, shown on Fig. 3, all internals were modeled in detail. No porous body approach was applied. All the 193 orifices in the core support plate were modeled. The perforated drum in the lower plenum was modeled and contains 410 orifices of 15 mm diameter. The core contains 193 fuel element dummies with a diameter of d=30 mm. The fluid flows through the hydraulic core simulator inside the tubes. The core can be modeled as free flow field; it is not expected to affect significantly the mixing in the lower plenum. This was done in the production mesh (grid 1). However, the core was modeled in detail in grid 2.

The influence of the outlet boundary position on the flow field and mixing in the downcomer and lower plenum is negligible. Nevertheless for completeness, the upper plenum and the outlet nozzles were modeled in detail in grid 2.

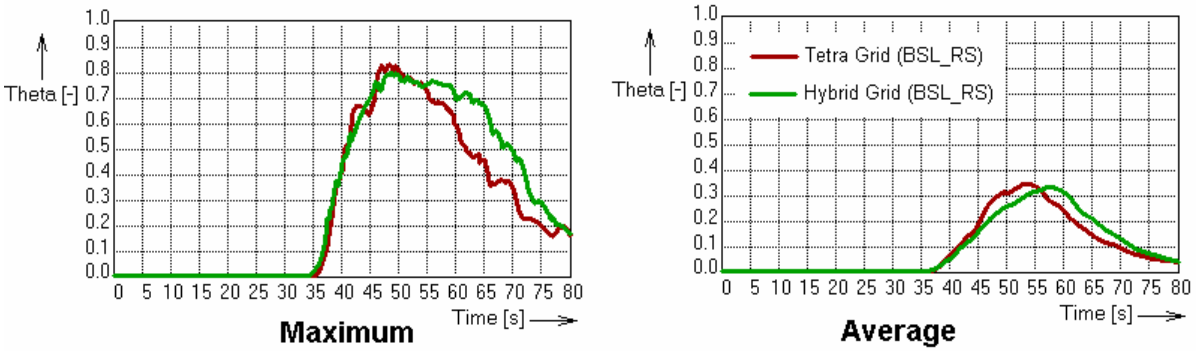

Fig. 4: Results of the maximum and averaged mixing scalar at the core inlet for both production meshes based on tetrahedral elements and hybrid elements

Tab. 2: Comparison of different grid types

Grid	Type	Size	Remarks
1	Tetrahedra	7 10^6 elements, 1.33 10^6 nodes	Perforated drum with original number of holes outlet at half of core tetrahedral production mesh
2	HYBRID	4.6 10^6 elements, 2.6 Mio. nodes Tetrahedra: 2.3 10^6 Pyramids: 29000 Hexahedra: 1.8 10^6 Wedges: 0.5 10^6	Perforated drum with original number of holes outlet at outlet nozzles hybrid production mesh

4.1.2 Time-step size

Sensitivity tests were made for time-step size. The time step size of 1.0 s (at t=20 s RMS Courant Number CFL=18.27) and 0.1 s (at t=20 s RMS Courant Number CFL=1.83) was used for 100 s simulation time (Fig. 5). Only small differences were observed.

4.1.3 Turbulence model

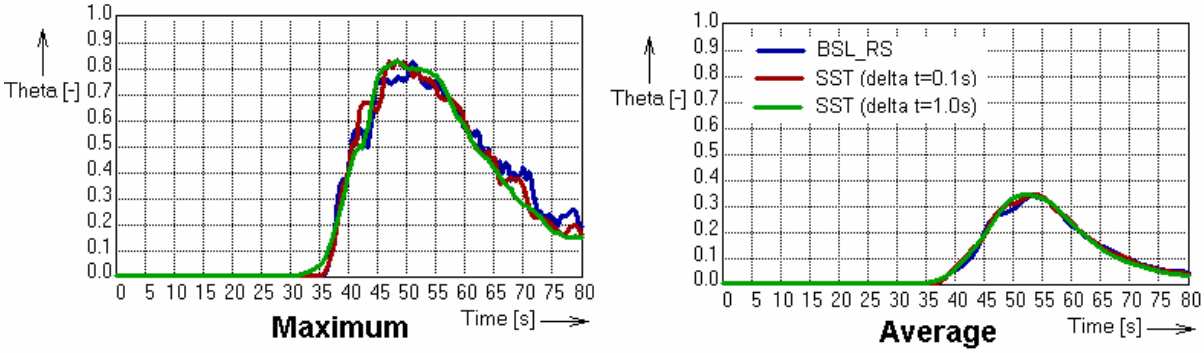

Fig. 5 Results of the maximum and averaged mixing scalar at the core inlet for time step variations and different turbulence models

Model errors should be evaluated only after solution errors have been quantified. As described above, quantification of discretisation errors was not possible to perform due to limited computer resources. The turbulence model is responsible for the quite dominating part of the model errors. Two types were used: the two-equation model SST and a Reynolds stress model. The SST model (Menter, 1993) works by solving a turbulence/frequency-based model (k–ω) at the wall and k-ε in the bulk flow. A blending function ensures a smooth transition between the two models. In the latter case the Reynolds stress model proposed by Launder (1975), which is based on the Reynolds Averaged Navier-Stokes Equations (RANS), was used in combination with an ω-based length scale equation (BSL model) to model the effects of turbulence on the mean flow. Fig. 5 shows only small differences between the SST and the BSL Reynolds stress (BSL_RS) turbulence model. So, the influence of the choice of the turbulence model is rather small.

4.1.4 Discretization schemes

All transient calculations were done with the higher order scheme "High Resolution" in space and "Fully implicit 2nd order backward Euler" in time. For both discretization schemes the target variable does not change any more for convergence criteria below 1×10^{-4}. Therefore this convergence criterion is used for all calculations. Double precision was used.

4.2 Boundary Conditions

The inlet boundary conditions (velocity, mixing scalar etc.) were set at the inlet nozzles. Transient experimental values of the mixing scalar were used. No specific velocity profile is given. As an initial guess of the turbulent kinetic energy and the dissipation rate the code standard is used. The outlet boundary conditions were pressure controlled. Passive scalar fields were used to describe the coolant mixing processes (Höhne, 2006).

Four transient calculations with 100s simulation time were performed on the FZD LINUX cluster (Operating system: Linux Scientific 64 bit, 32 AMD OPTERON Computer Nodes, Node configuration: 2 x AMD OPTERON 285 (2.6 GHz, dual-core), 16 GB Memory) and they took 9 days each to complete. Six processors were used for the above mentioned simulations in a parallel mode with the message passing protocol PVM.

5. RESULTS

5.1 Qualitative comparison of experimental and calculation results

Based on the above described sensitivity studies the hybrid grid with the smaller time step and the SST turbulence model has been selected for the direct comparison with the experimental results. Fig. 6 contains snapshots of the distribution of the measured and calculated mixing scalar in the downcomer at three different time points. It can be seen that in the experiment and in the calculation the slugs enter the highest measurement plane at three positions nearly at the same time. Velocity measurements using laser Doppler anemometry revealed an unequal azimutal velocity distribution with four maxima in-between the leg nozzles during four loop operation mode (Rohde, 2005). This distribution is responsible for the observed scalar field. The calculation reproduces this velocity field and therefore also the distribution of the mixing scalar. The second snapshot (t = 40.0 s) demonstrates that the transport of the tracered water in radial direction in the upper part of the downcomer is quite limited. It also confirms the quality of the mass flow boundary conditions in the experiment. The tracer covers a 180 ° sector in the uppermost line which corresponds to the share of the mass flow rate of the two loops with slugs. Both in the experiment as well as in the calculation two positions with very low velocity can be observed in this snapshot (tracer-free regions). In the calculation these regions are located somewhat lower than in the experiment. From the third experimental snapshot (t = 50.0 s) can be concluded that the transport of the tracer in radial direction starts in the lower part of the downcomer (widening of the sector covered by tracer). For some reason in the calculation this effect is to be seen only at one side of the slugs.

Fig. 6 contains also the measured and calculated tracer distribution in the core inlet plane at the time point of the maximum of the mixing scalar. The distribution is shown as isolines of the mixing scalar. The position and the value of the maximum are indicated. The measurement shows three region with nearly identical values, the maximum itself belongs to the region in-between the loop positions where the slugs started. Such a distribution means that during the moving of the slugs through the downcomer the shape of the tracer field has not been changed. The isolines indicate a smooth distribution of the mixing scalar. In the calculation the mixing scalar is distributed much more non-uniform. The two maxima in the outer edges are more expressed than those in the middle between the loop positions. For that reason, the position of the calculated maximum is in one of these outer regions.

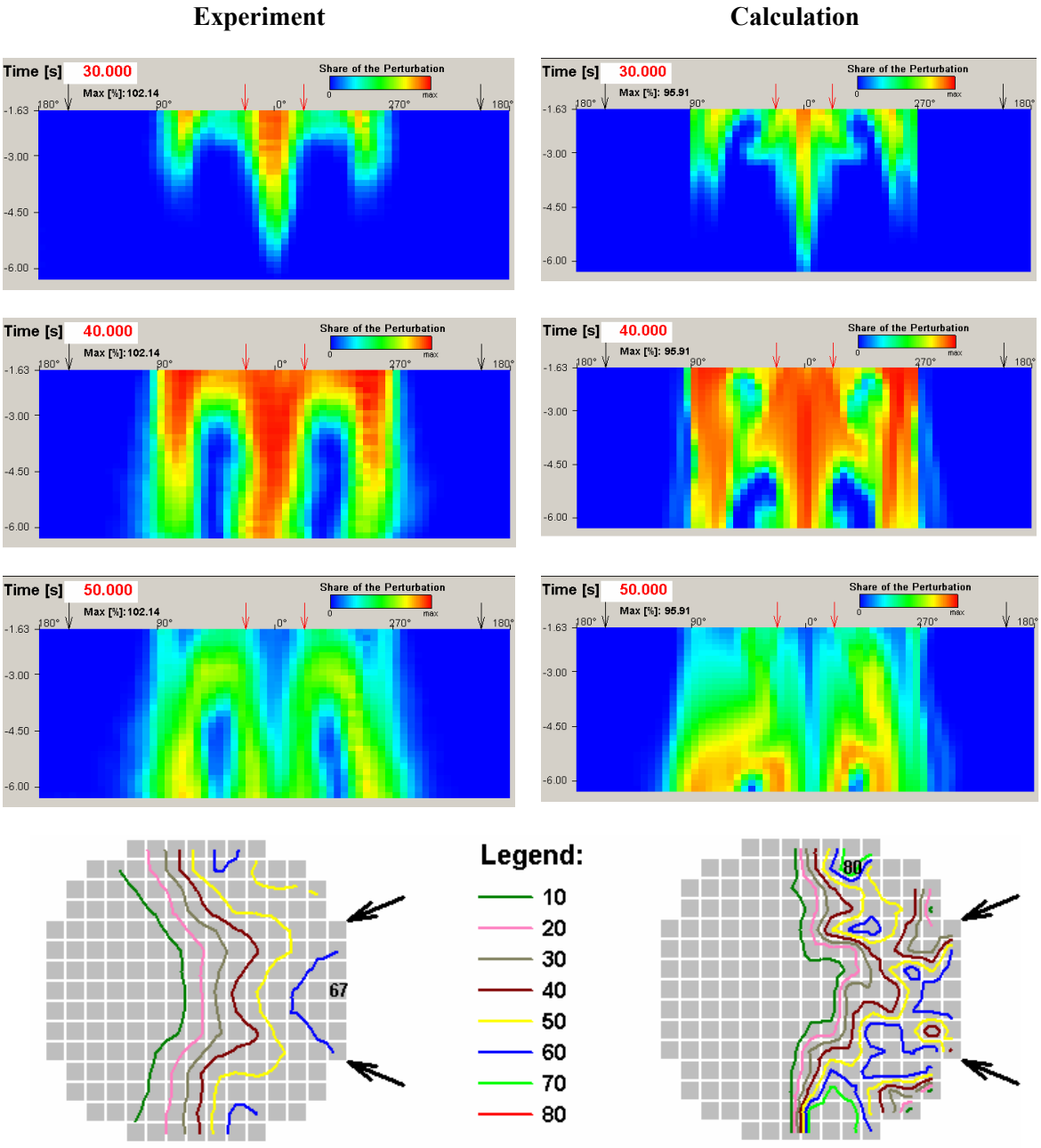

Fig. 6: Snapshots of mixing scalar distribution in the downcomer at three time points and in the core inlet plane at the time of maximum

5.2 Quantitative comparison of experimental and calculation results

The values of the single realisations of the experiment were used to determine time-dependent confidence intervals of the measurement data. This is done according to the following procedure (Kliem, 2008): In the first step, the minimum error amount $FS_{min,\Theta}$ for each local value of the mixing scalar at each time point is calculated according to Eq. (3), using the averaged values and the n single realizations:

$$FS_{\min,\Theta}(x,y,z,t) = \sum_{k=1}^{n} (\theta_{ROCOM,k}(x,y,z,t) - \bar{\theta}_{ROCOM}(x,y,z,t))^2 \tag{3}$$

The standard deviation is calculated according to

$$s_{\Theta}(x,y,z,t) = \sqrt{\frac{FS_{\min,\Theta}(x,y,z,t)}{n-1}} \tag{4}$$

In the last step, the confidence intervals can be calculated using:

$$u_{z,\Theta}(x,y,z,t) = \pm t_P . \frac{s_{\Theta}(x,y,z,t)}{\sqrt{n}} \tag{5}$$

This confidence interval characterizes the interval around the average value in which the measured value can be found with a given probability of the statistical confidence. Hereby, t_p is the value of the Student's t-factor, which varies with the selected statistical confidence. Usually, the confidence intervals for 68.4 % (corresponds to 1 σ), for 95.4 % (2 σ) and 99.5 % (3 σ) are calculated and included in the documentation, whereby σ is the square root of the variance of the distribution.

The time curves of the confidence intervals for 1 σ (p1) and 2 σ (p2) are included in each of the following figures. Fig. 7 shows the time history of the maximum and the average mixing scalar in the downcomer sensor. The calculated average mixing scalar always belongs to the confidence interval of one standard deviation. The calculation underestimates the maximum of the mixing scalar in the downcomer, around the time of the maximum the calculated value belongs to the p2 confidence interval.

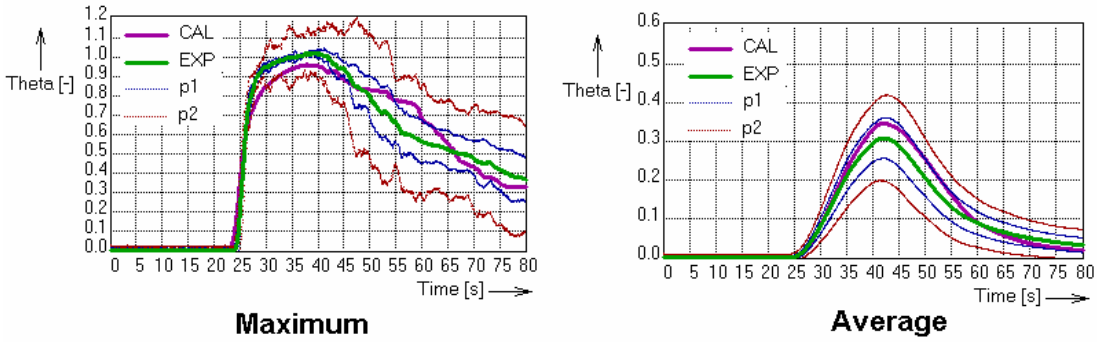

Fig. 7: Maximum and averaged mixing scalar in the downcomer (Comparison between experiment and calculation including confidence interval of the experimental data)

The underestimation is clearly a result of the used boundary conditions. For the calculation the measured time history in the inlet nozzle averaged over the cross section was used. Improvements are expected when the cold legs until the initial position of the slugs are included into the calculation domain, what is foreseen for the near future.

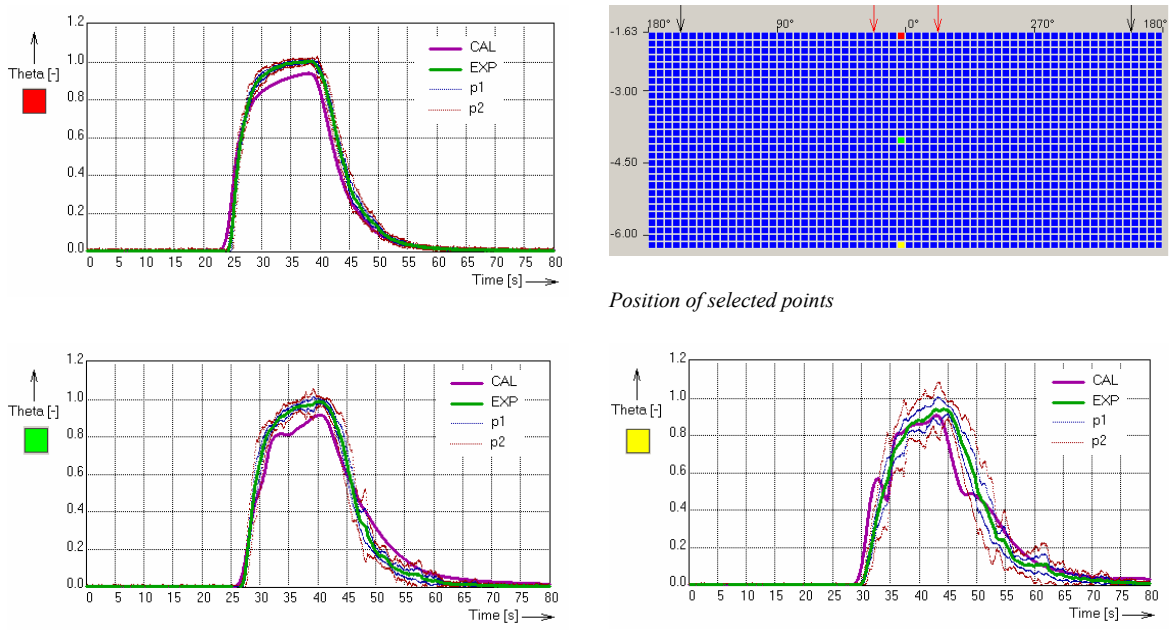

Fig. 8: Comparison between experiment and calculation at three measurement positions in the downcomer (including confidence interval of the experimental data)

Fig. 8 presents the direct comparison between measurement and calculation at three single positions in the downcomer, On the right hand side, the scheme of the measurement grid in the downcomer is shown with the azimutal positions of the four loops (the red arrows indicate the loops with the slugs). The three positions have been selected on the middle line between the two loops with the slugs. Again, the confidence intervals are shown, too. It can be seen how the confidence intervals are widening with increasing distance from the inlet into the downcomer. This is an indication for the increase of the turbulent fluctuations. The calculated time history of the mixing scalar around the time of the maximum in the two uppermost selected positions is outside (below) the confidence interval due to its small width. At the lowest position, the calculated time history belongs most of the time to the p1 confidence interval. Besides the mentioned widening of the confidence interval, this agreement has the following reason. As mentioned above, the calculation does not take into account the spatial distribution of the mixing scalar in the inlet nozzle. Due to the use of the average curve, the calculated mixing scalar is smaller than the measured one in the selected position. With increasing distance the measurement shows a higher mixing (sharper decrease of the mixing scalar) than the calculation. The combination of a lower starting value with a smaller mixing effect leads to the observed convergence.

Tab. 3: Comparison of the calculated mixing scalars in the downcomer with the confidence intervals

	Confidence interval		
	p1	**p2**	**p3**
Maximum value	438	764	860
Time point of maximum	595	887	983
Combined (value and time point)	255	652	792
Total number of assessed positions	1106		

Tab. 3 shows a quantitative comparison of the downcomer measurement data with the calculation. In each cell the number of positions in the calculation is shown which belongs to the corresponding experimentally determined confidence interval. The maximum value reached at each position, the time point of reaching this maximum value and the combination (so-called two-dimensional confidence intervals) are assessed. Assessment has been carried out not for all 1856 single measurement positions in the downcomer but for those of them receiving a mixing scalar of at least 10 % (1106 positions). From the table can be seen that the calculated maximum value fits into the two-dimensional confidence interval of one standard deviation at 255 positions (~23 %).

In the core inlet plane (Fig. 9), the calculated average mixing scalar is even in better agreement than in the downcomer. Contrary to this agreement the calculation overestimates the maximum value. Due to the time lag between reaching the maximum in measurement and calculation the calculated maximum value is partly outside of the p2 confidence interval. The measurement shows a remarkable reduction of the mixing scalar during the transport through the lower plenum as can be concluded by comparing data in the outlet plane of the downcomer sensor and in the core inlet plane. The calculation shows only a small reduction for the same flow path. The tendency of underestimation of mixing in the downcomer found by the comparison of the detailed downcomer data is valid also for the lower plenum.

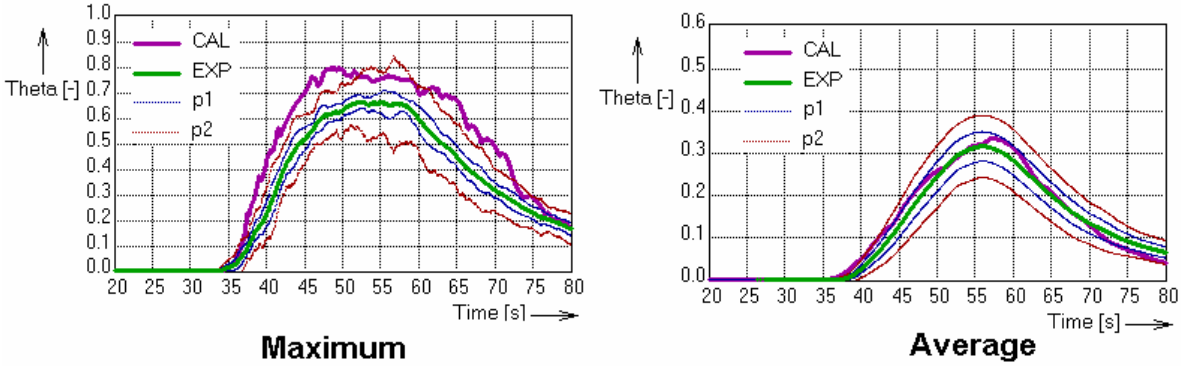

Fig. 9: Maximum and averaged mixing scalar at the core inlet (Comparison between experiment and calculation including confidence interval of the experimental data)

Due to the very complex flow pattern at the end of the downcomer and in the lower plenum, the existence of the perforated sieve drum with the 410 orifices for instance and the core inlet plate and the 180° flow direction change, the agreement of the CFX calculation and the experiment at the core inlet is smaller than at the upper part of the downcomer. It is expected that these deviations can be reduced by using a finer mesh since the used one is not solution independent, especially in regions with high velocity gradients. As the grid is already very large and complex, this topic is subject for future research generating grids larger than 20 million cells using massive parallel computations.

6 CONCLUSIONS

A coolant mixing experiment with boundary conditions based on a SBLOCA scenario carried out at the ROCOM test facility has been used for the validation of the CFD code ANSYS CFX. The data of the new downcomer sensor spanning a very dense grid of nearly 1900 measurement positions were used for a detailed comparison between measurement and calculation. This comparison shows a good qualitative agreement. All main effects observed in the measurement are described by the calculation. The detailed comparison reveals that the CFD solution underestimates the coolant mixing inside the RPV. The calculated mixing scalar values are higher than the measured ones especially in the core inlet plane. The calculation used for this comparison was derived during a sensitivity study using the best practice guidelines.

The measurement data, boundary conditions of the experiment and facility geometry can be made available for further CFD code benchmarking. The experimental data comprise measurement values of the dimensionless tracer concentration at all sensor positions for single realizations of the test or averaged over all test runs.

REFERENCES

CFX11 (2007), User Manual, ANSYS-CFX

Hertlein, R., Umminger, K., Kliem, S., Prasser, H.-M., Höhne, T., Weiss, F.-P. (2003), Experimental and numerical investigation of boron dilution transients in pressurized water reactors, Nuclear Technology, vol. 141, pp. 88-107

Höhne, T., Kliem, S., Bieder, U. (2006), Modeling of a buoyancy-driven flow experiment at the ROCOM test facility using the CFD-codes CFX-5 and TRIO_U, Nucl. Eng. Design, vol. 236, pp. 1309-1325

Hyvärinen, J. (1993), The Inherent Boron Dilution Mechanism in Pressurized Water Reactors, Nucl. Eng. Des., 145, pp. 227-340

Kliem, S., Hemström, B., Bezrukov, Y., Höhne, T., Rohde, U. (2007), Comparative Evaluation of Coolant Mixing Experiments at the ROCOM, Vattenfall, and Gidropress Test Facilities, Science and Technology of Nuclear Installations, vol. 2007, Article ID 25950, 17 p., doi:10.1155/2007/25950

Kliem, S., Sühnel, T., Rohde, U., Höhne, T., Prasser, H.-M., Weiss, F.-P. (2008), Experiments at the mixing test facility ROCOM for benchmarking of CFD codes, Nucl. Eng. Design, vol. 238, pp. 566-576

Kliem, S., Prasser, H.-M., Sühnel, T., Weiss, F.-P., Hansen, A. (2008a), Experimental determination of the boron concentration distribution in the primary circuit of a PWR after a postulated cold leg small break loss-of-coolant-accident with cold leg safety injection, Nucl. Eng. Design, vol. 238, pp. 1788-1801

Launder, B. E., Reece, G. J., Rodi, W. (1975), Progress in the development of a Reynolds-stress turbulence closure, J. Fluid Mech. Vol. 68, pp. 537-566

Menter, F. (1993), Zonal Two Equation k-ω Turbulence Models for Aerodynamic Flows, AIAA Paper 93-2906

Menter, F. (2002), CFD Best Practice Guidelines for CFD Code Validation for Reactor Safety Applications, ECORA FIKS-CT-2001-00154

Mull, Th. and Umminger, K. (2003), New PKL-tests on boron dilution in PWRs, Annual Meeting on Nuclear Technology '03, Proc. Topical Session: "Experimental an theoretical investigations on boron dilution transients in PWRs", pp. 23-56, INFORUM GmbH Berlin, Germany

Prasser, H.-M., Böttger, A., Zschau, J. (1998), A new electrode-mesh tomograph for gas-liquid flows, Flow Measurement and Instrumentation, vol. 9, pp. 111-119

Prasser, H.-M., Grunwald, G., Höhne, T., Kliem, S., Rohde, U., Weiss, F.-P. (2003), Coolant mixing in a PWR - deboration transients, steam line breaks and emergency core cooling injection - experiments and analyses, Nuclear Technology, vol. 143, pp. 37-56

Rohde, U., Kliem, S., Höhne, T., Karlsson, R. et al. (2005), Fluid mixing and flow distribution in the reactor circuit: Measurement data base, Nucl. Eng. Design, vol. 235, pp. 421-443

Rohde, U., Höhne, T., Kliem, S., Hemström, B. et al. (2007), Fluid mixing and flow distribution in the reactor circuit – Computational fluid dynamics code validation, Nucl. Eng. Design vol. 237, pp. 1639-1655